

REPORT DOCUMENTATION PAGE			<i>Form Approved</i> OMB No. 0704-0188		
Public reporting burden for this collection of information is estimated to average 1 hour per response, including the time for reviewing instructions, searching existing data sources, gathering and maintaining the data needed, and completing and reviewing this collection of information. Send comments regarding this burden estimate or any other aspect of this collection of information, including suggestions for reducing this burden to Department of Defense, Washington Headquarters Services, Directorate for Information Operations and Reports (0704-0188), 1215 Jefferson Davis Highway, Suite 1204, Arlington, VA 22202-4302. Respondents should be aware that notwithstanding any other provision of law, no person shall be subject to any penalty for failing to comply with a collection of information if it does not display a currently valid OMB control number. PLEASE DO NOT RETURN YOUR FORM TO THE ABOVE ADDRESS.					
1. REPORT DATE (DD-MM-YYYY) 11-04-2011		2. REPORT TYPE Article		3. DATES COVERED (From - To) MAR 2011 - APR 2011	
4. TITLE AND SUBTITLE The Hydrophobicity and Adhesion of Heterogeneous Surfaces of Dual Nanometer and Micron Scale Structures*			5a. CONTRACT NUMBER FA8720-05-C-0002		
			5b. GRANT NUMBER		
			5c. PROGRAM ELEMENT NUMBER		
6. AUTHOR(S) Shaun Berry, Theodore Fedynyshyn, Lalitha Parameswaran and Alberto Cabral			5d. PROJECT NUMBER		
			5e. TASK NUMBER		
			5f. WORK UNIT NUMBER		
7. PERFORMING ORGANIZATION NAME(S) AND ADDRESS(ES) MIT Lincoln Laboratory 244 Wood Street Lexington, MA 02420			8. PERFORMING ORGANIZATION REPORT NUMBER		
9. SPONSORING / MONITORING AGENCY NAME(S) AND ADDRESS(ES) AFLCMC/PZE 20 Schilling Circle, Bldg 1305 Hanscom AFB, MA 01731			10. SPONSOR/MONITOR'S ACRONYM(S) AFLCMC/PZE		
			11. SPONSOR/MONITOR'S REPORT NUMBER(S)		
12. DISTRIBUTION / AVAILABILITY STATEMENT DISTRIBUTION STATEMENT A. Approved for public release; distribution is unlimited.					
13. SUPPLEMENTARY NOTES					
14. ABSTRACT An investigation was performed to study the effect a heterogeneous surface consisting of nanometer scale square posts patterned into micron scale checkerboard shapes had on surface hydrophobicity and water adhesion. In addition to altering surface geometries, different surface coatings were investigated. Conformal thin films of PDMS, CYTOP, and Teflon AF were made using a surface grafting technique and applied to each nano-scale and micro-scale design fabricated for this study. Both the static contact angle and the tilt angle required for a water drop to roll-off the surface were measured to determine the wetting state for a particular surface geometry. For nano-scale posts with spacing-to-width ratios below a certain threshold value, patterned into micro-scale checkerboard shapes with a spacing-to-width ratio < 1, the hydrophobicity of a surface was increased compared to a surface made of either all nano-scale features or all micro-scale features. Conversely, as the spacing-to-width ratio of the nano-scale square posts increased above the threshold value, for the micro-scale checkerboard shapes having a spacing-to-width ratio 5:1 the surface hydrophobicity was reduced and water adhesion increased compared to a surface made of either all nano-scale features or all micro-scale features. The nano-scale spacing-to-width ratio threshold value that caused this behavior to occur was dependent on both post width and surface coating. Finally it was observed, that for the micro-scale checkerboard shapes having a spacing-to-width > 1, the micro-scale features dominated the wetting state regardless of the nano-scale post geometry.					
15. SUBJECT TERMS superhydrophobic, surface modification, adhesion, contact angle, Cassie, Wenzel, PDMS, CYTOP, Teflon AF, roll-off angle					
16. SECURITY CLASSIFICATION OF: U			17. LIMITATION OF ABSTRACT SAR	18. NUMBER OF PAGES 26	19a. NAME OF RESPONSIBLE PERSON Zach Sweet
a. REPORT U	b. ABSTRACT U	c. THIS PAGE U			19b. TELEPHONE NUMBER (include area code) 781-981-5997

The Hydrophobicity and Adhesion of Heterogeneous Surfaces of Dual Nanometer and Micron Scale Structures*

Shaun Berry, Theodore Fedynyshyn, Lalitha Parameswaran and Alberto Cabral*

MIT Lincoln Laboratory, 244 Wood St. Lexington, MA 02420

sberry@ll.mit.edu

RECEIVED DATE

THIS MATERIAL HAS BEEN CLEARED
FOR PUBLIC RELEASE BY 66 ABW/PA

DATE:

11 Apr 11

CASE #

66ABW-2011-0416

ABSTRACT An investigation was performed to study the effect a heterogeneous surface consisting of nanometer scale square posts patterned into micron scale checkerboard shapes had on surface hydrophobicity and water adhesion. In addition to altering surface geometries, different surface coatings were investigated. Conformal thin films of PDMS, CYTOP, and Teflon AF were made using a surface grafting technique and applied to each nano-scale and micro-scale design fabricated for this study. Both the static contact angle and the tilt angle required for a water drop to roll-off the surface were measured to determine the wetting state for a particular surface geometry. For nano-scale posts with spacing-to-width ratios below a certain threshold value, patterned into micro-scale checkerboard shapes with a spacing-to-width ratio ≤ 1 , the hydrophobicity of a surface was increased compared to a surface made of either all nano-scale features or all micro-scale features. Conversely, as the spacing-to-width ratio of the nano-scale square posts increased above the threshold value, for the micro-scale checkerboard shapes

*This work was sponsored by the Department of the Air Force under Air Force Contract FA8721-05-C-0002. Opinions, interpretations, conclusions, and recommendations are those of the authors, and do not necessarily represent the view of the United States Government.

having a spacing-to-width ratio ≤ 1 the surface hydrophobicity was reduced and water adhesion increased compared to a surface made of either all nano-scale features or all micro-scale features. The nano-scale spacing-to-width ratio threshold value that caused this behavior to occur was dependent on both post width and surface coating. Finally it was observed, that for the micro-scale checkerboard shapes having a spacing-to-width > 1 , the micro-scale features dominated the wetting state regardless of the nano-scale post geometry.

KEYWORDS superhydrophobic, surface modification, adhesion, contact angle, Cassie, Wenzel, PDMS, CYTOP, Teflon AF, roll-off angle

Introduction

The use of textured surfaces to achieve superhydrophobicity can be routinely found in nature. For example, many plant leaves^{1,2}, bird feathers³, insect wings and insect legs⁴ take advantage of micron and/or nanometer scale features to modify the wetting state. The best known example is the lotus plant, which has leaves that exhibit superhydrophobic, self-cleaning properties where water beads up into droplets and easily rolls off the leaves' surfaces. These leaves have a double structure of micron sized nubs about 20-40 μm with nano-scale asperities superimposed and coated with a waxy layer for increased hydrophobicity⁵. Interestingly, the rose petal is also made up of dual micro and nano-scale structures of roughly the same scale as the lotus leaf, but its structures are arranged in such a way to allow water to bead up into droplets but instead of rolling off, adhere to the surface, giving the petal a fresh look². Artificially fabricated hierarchy structures of micro-scale and superimposed nano-scale features have been built by many groups and it has been shown these structures can be engineered to be non-wetting with high water contact angles and small contact angle hysteresis^{1,6-9}. It should be noted that dual length scale structures are not a prerequisite for producing surfaces that exhibit superhydrophobic or superhydrophilic wetting behavior. Regularly patterned micron sized structures only¹⁰⁻¹³, nano-sized structures only¹⁴⁻¹⁷, and chemical surface modifications¹⁸ have been demonstrated to enhance the wetting state of a surface to produce superhydrophobic characteristics.

The majority of the past work associated with hierarchy structures with regularly patterned dual length scale features has been based on a continuous pattern of micron features overlaid with a continuous pattern of nano-scale features, meaning the nano-scale features sit on top of the micron features. Unique in this work, we report on the wettability of heterogeneous surfaces consisting of nanometer scale square posts that were patterned into micron scale checkerboard shapes. This was accomplished by etching nano-scale structures into silicon and then removing sections of the structures to form discrete micro-scale groups. This communication will present the results from a comprehensive study investigating the wetting properties of different combinations of nano-scale and micro-scale geometries. In addition to different geometries, we also evaluated three different organic hydrophobic films, Polydimethylsiloxane (PDMS), CYTOP and Teflon AF to study the effect the surface energy had on the wetting state for a fixed geometry. A surface grafting process was used to create a conformal thin film on our structures. Both equilibrium water contact angle and the minimum angle in which a drop would roll-off the surface were measured in order to fully characterize the wetting state of a particular surface.

Experimental Section

Design. Three different categories of features were fabricated; nano-scale only, micro-scale only and combined nano- and micro-scale. Table 1 and Table 2 highlight the dimensions of the nano-scale features and micro-scale features respectively. The nano-scale features fabricated were arrays of square posts with widths, $w = 400\text{nm}$, 600nm and 1000nm . For each post width three different spacing-to-width ratios were studied, $d/w = 1:1$, $2:1$, and $3:1$ where d is the spacing between posts. The micro-scale pattern investigated was a checkerboard pattern. Two different checkerboard sizes were studied and for each checkerboard size there were five different spacing-to-width ratios (b/a) evaluated, where b is the distance between features along a given row or column of features and a is the width of the feature. Checkerboard features with $b/a < 1$ created square pockets on the surface and for $b/a > 1$ created isolated islands of features on the surface. For combined nano-scale and micro-scale features, continuous surfaces of the nano-scale posts were first made per dimensions listed in Table 1 and then

patterned into micro-sized checkerboard shapes per dimensions listed in Table 2. In this study only a single feature height of $h = 2 \mu\text{m}$ was evaluated for all categories of features due to aspect ratio concerns.

Table 1. Features and sizes of the of the nano-scale structures on the nano-scale test mask. “Name” is the common name for the nano-scaled feature, w is the feature width in nanometers, d is the distance between features in nanometers. d/w is the spacing-to-width ratio.

Name	w (nm)	d (nm)	d/w
Posts-1000/1000	1000	1000	1
Posts-600/600	600	600	1
Posts-400/400	400	400	1
Iso Posts-2000/1000	1000	2000	2
Iso Posts-3000/1000	1000	3000	3
Iso Posts-1200/600	600	1200	2
Iso Posts-1800/600	600	1800	3

Table 2. Features and sizes of the of the micro-scale structures on the micro-scale test mask. “Name” is the common name for the micro-scaled feature, a is the feature width in micrometers, b is the distance between features in micrometers. b/a is the spacing-to-width ratio.

Name	a (μm)	b (μm)	b/a
Checkerboard-1 20/60	60	20	0.33
Checkerboard-2 20/40	40	20	0.5
Checkerboard-3 20/20	20	20	1
Checkerboard-4 40/20	20	40	2
Checkerboard-5 60/20	20	60	3
Checkerboard-6 50/150	150	50	0.33
Checkerboard-7 50/100	100	50	0.5
Checkerboard-8 50/50	50	50	1
Checkerboard-9 100/50	50	100	2
Checkerboard-10 150/50	50	150	3

Fabrication. Individual and combined nanometer and micron sized features were created by first depositing 500 nm of plasma-enhanced chemical vapor deposition (PECVD) silicon dioxide on a 150-mm diameter silicon wafer. Next the nano-scale features were patterned using a 248nm Canon FPA-3000 EX4 Stepper with an exposure dosage of 150 J/m^2 . The oxide was then thru-etched using a dry-etch process creating the nano-sized features in the oxide. The photoresist was stripped using oxygen

plasma to avoid damaging the nano-scale structures. Next, the micron features were patterned using a Canon FPA 3000 iW i-line stepper. After exposure the resist was developed manually by placing the wafer in a bath containing the developer and agitating gently allowing the developer to wash over the wafer surface slowly to avoid breaking the nano-scale structures. The oxide was then thru-etched using a dry etch process creating the micron sized features. The photoresist was then stripped using oxygen plasma.

Using the oxide film as a hard mask, both the nano-scale and micron features were etched into the silicon simultaneously employing a Plasmatherm ICP Bosch (Versalock-700). The tool was operated in a non-Bosch mode to create features with smooth vertical side walls. After the silicon etch the oxide hard mask was stripped using a dry-etch process. The etch depth was then measured using a KLA-Tencor P-10 profilometer and found to be 2 μm . The wafer was then cleaned in Piranha, followed by a cascade deionized water rinse. Next, 50 nm of thermal oxide was grown over the silicon surface and then cleaned with Piranha to prepare the oxide for additional surface modification. Figure 1 shows scanning electron microscopy images of selected combined nano-scale and micro-scale structures taken at different magnifications.

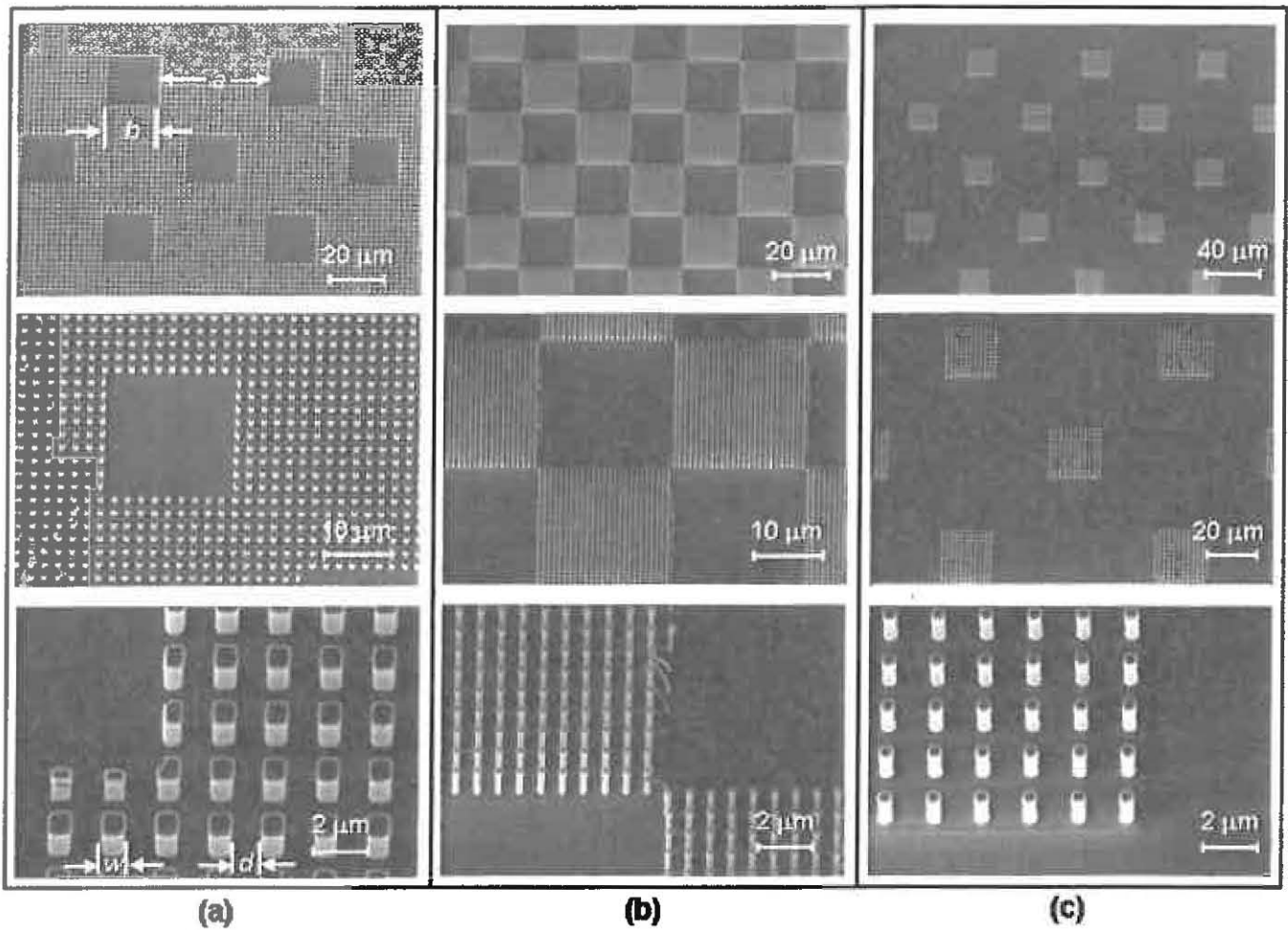


Figure 1. Scanning electron microscopy images taken at different magnifications. (a) Images of the combined nano-scale feature: Post 1000/1000, $d = 1000\text{nm}$, $w = 1000\text{nm}$ and the micro-scale feature: Checkerboard-1 20/40, $b = 20\mu\text{m}$, $a = 40\mu\text{m}$. (b) Images of the combined nano-scale feature: Posts 400/400, $d = 400\text{nm}$, $w = 400\text{nm}$ and the micro-scale feature: Checkerboard-3 20/20 $b = 20\mu\text{m}$, $a = 20\mu\text{m}$. (c) Images of the combined nano-scale feature: Iso Posts-1200/600, $d = 1200\text{nm}$, $w = 600\text{nm}$ and the micro-scale feature: Checkerboard-5 60/20, $b = 60\mu\text{m}$, $a = 20\mu\text{m}$.

Surface Modification. To enhance the hydrophobicity of the structured surface, individual surfaces were coated with a hydrophobic film. Three different organic hydrophobic films were investigated, Polydimethylsiloxane (PDMS) and two fluoropolymers; CYTOP grade 809M (Ashai Glass Co.) and

Teflon AF1601 (Du Pont). A surface grafting process which creates a covalently attached polymer was used to produce a conformal coating for each film.

PDMS: 1000cSt PDMS was spun at 1000 RPM for 1 min. After spinning, the material was soft baked at 120°C for 5 min and then hard baked at 220°C on a hot plate for 1 hour. After baking, the non-grafted PDMS was stripped by submerging the surface in a bath of hexane for 24 hours. The resulting conformal layer was measured by ellipsometer to be between 6nm and 10nm. The contact angle of a deionized (DI) water drop on a planar surface of this film measured 105°.

CYTOP: 9% CYTOP was spun at 550 RPM for 1 min. After spinning, the material was soft baked at 120°C for 5 min and then hard baked at 220°C on a hot plate for 1 hour. After baking the non-grafted CYTOP was stripped by submerging the surface in a bath of FC-40 (3M) for 24 hours. The resulting conformal layer was measured to be between 10nm and 15nm. The contact angle of a DI water drop on a planar surface of this film measured 116°.

Teflon AF: Teflon AF1601 was spun at 550 RPM for 1 min. After spinning, the material was soft baked at 120°C for 5 min and then hard baked at 220°C on a hot plate for 1 hour. After baking the non-grafted Teflon AF was stripped by submerging the surface in a bath of FC-40 for 24 hours. The resulting conformal layer was measured to be between 10nm and 15nm. The contact angle of a DI water drop on a planar surface of this film measured 122°.

Contact Angle Measurements. Contact angle data was collected for each individual and combined nano- and micro- scaled feature and hydrophobic film type. All contact angles reported were measured in an air ambient. A 10 μ L sessile drop of DI water was dispensed on the center of the surface containing the test feature and the apparent contact angle at the three-phase contact line was measured using a Ramé-Hart model 200 goniometer with DROPimage Advance imaging software.

Roll-off Angle Measurements. The roll-off angle was measured by first securing the test surface on a 75mm x 50mm aluminum plate. Next a 10 μ L sessile drop of DI water was dispensed on the center of the surface containing the test feature. The plate containing the test surface and drop was tilted with a linear actuator (Newport 850b, 25mm stroke, 0-1mm/s) by pushing vertically upward on the bottom of

the plate at one end while keeping the other end hinged. The height at which the drop began to roll was recorded. Since the horizontal distance between the hinge point and liner actuator was constant, the roll-off angle could be determined once the stroke height was measured. The angle measurement was repeated a minimum of three times for each feature tested. The stroke limit of the actuator and practical constraints on its placement relative to the hinge point only allowed a maximum tilt of 45°. Once a test reached the stroke limit, the plate was manually rotated through 90°. If the drop stayed on the surface at 90° it was classified as being pinned, if it rolled prior to 90° but was greater than 45° it was classified as >45°. Less than 45° the actual angle was recorded.

Results and Discussion

Table 3 shows the contact angle data for structures fabricated and coated with PDMS, CYTOP and Teflon AF for the three categories of features: micro-scale-only features (column called “No Nano”), nano-scale-only features (row called “No Micron”) and combined nano- and micro-scale. The contact angle value measured for the “No Micron” and “No Nano” case is for a planar surface of the grafted hydrophobic film. During the measurements it was found the repeatability of the contact angle for any given feature was within $\pm 3^\circ$. The dark grayed areas in the table highlight contact angles $\geq 150^\circ$, which is considered one of the conditions for a surface being superhydrophobic²⁰.

Table 3. Measured contact angle values in degrees for PDMS, CYTOP and Teflon AF coated individual and combined nano-scale and micro-scale features. Grayed areas indicate contact angles $\geq 150^\circ$.

		Nano-scale Features (d/w)																									
		PDMS								CYTOP								Teflon AF									
		No Nano	Posts (1000/1000)	Iso Posts (2000/1000)	Iso Posts (3000/1000)	Posts (600/6000)	Iso Posts (1200/600)	Iso Posts (1800/600)	Posts (400/400)	No Nano	Posts (1000/1000)	Iso Posts (2000/1000)	Iso Posts (3000/1000)	Posts (600/6000)	Iso Posts (1200/600)	Iso Posts (1800/600)	Posts (400/400)	No Nano	Posts (1000/1000)	Iso Posts (2000/1000)	Iso Posts (3000/1000)	Posts (600/6000)	Iso Posts (1200/600)	Iso Posts (1800/600)	Posts (400/400)		
Micro-Scale Features (h/a)	No Micron	105	120	147	131	123	155	135	124	116	153	156	129	139	157	135	154	123	154	150	159	160	151	161	153		
	Checkerboard-1 (20/60)	112	149	158	124	151	156	133	153	119	159	158	129	158	159	160	163	126	149	156	137	160	158	161	154		
	Checkerboard-2 (20/40)	115	146	132	122	151	146	127	148	125	155	159	128	160	159	135	159	129	157	157	135	160	157	165	157		
	Checkerboard-3 (20/20)	128	152	120	116	153	125	117	157	121	153	157	132	159	158	167	150	141	159	155	146	154	154	160	165		
	Checkerboard-4 (40/20)	116	116	114	112	117	114	111	118	121	125	119	116	127	125	118	124	127	130	129	122	132	132	122	132		
	Checkerboard-5 (60/20)	106	107	107	110	104	107	107	103	120	119	119	117	122	119	118	120	126	127	125	123	127	125	127	127		
	Checkerboard-6 (50/150)	109	151	152	125	151	152	135	154	137	154	120	118	160	148	118	159	128	161	153	126	160	154	131	163		
	Checkerboard-7 (50/100)	115	151	143	123	153	157	120	153	125	158	158	125	160	157	135	157	129	157	157	127	160	157	130	161		
	Checkerboard-8 (50/50)	132	147	122	113	155	136	115	150	138	158	132	115	160	158	122	157	142	158	159	129	160	161	133	164		
	Checkerboard-9 (100/50)	105	113	113	106	116	113	110	113	119	125	118	115	124	122	118	124	123	128	125	125	128	125	124	128		
	Checkerboard-10 (150/50)	105	112	107	108	111	108	110	111	117	117	118	114	123	120	118	120	125	128	126	123	125	128	123	129		

As the data in Table 3 highlights there were several geometries for the different hydrophobic films that produced high water contact angles of $\geq 150^\circ$.

However, a high contact angle does not necessarily mean that a surface is more hydrophobic than a surface having a lower measured contact angle. Recalling, that for textured surfaces there are two general equilibrium states for a drop of water; the Wenzel state²¹ or the Cassie-Baxter (Cassie) state²². In the Wenzel state liquid is in complete contact with surface, meaning the droplet fills all surface protrusions. In the Cassie state its assumed air stays trapped between the protrusions and the liquid sits on top a composite surface of air and solid. The theory for both states predicts that high contact angles can exists, and depending on the geometry (protrusion size, spacing and height) can exceed 150° for water. The principal difference between these two states is with the dynamic behavior a drop exhibits on the surface. A drop in a Cassie state will roll-off the surface more easily when the surface is tilted compared to a drop in a Wenzel state, which is often pinned to the surface or shows high contact angle hysteresis¹⁴.

Therefore static contact angle alone is not sufficient to establish the hydrophobicity of a surface. Oner *et. al.*^{19,20} asserts that contact angle hysteresis is a more accurate way to quantify the hydrophobicity of a surface. The smaller the contact angle hysteresis, which is the difference between the advancing (θ_{adv}) and receding contact angle (θ_{rec}) the easier it is for a drop to roll on the surface and therefore the higher the hydrophobicity. In this work θ_{adv} and θ_{rec} were not directly measured, except for the planar surfaces of the grafted films, instead the roll-off angle, ϕ , was measured. This was the minimum tilt angle required for a drop to begin to roll on the surface and is directly proportional to amount of contact angle hysteresis as governed by the following equation¹⁰

$$\frac{mg \sin \phi}{x} = \gamma (\cos \theta_{rec} - \cos \theta_{adv}) \quad (1)$$

where g is the gravitational acceleration, γ is surface tension of water, and m and x are the mass and width of the drop respectively. This relation implies the smaller the roll-off angle the smaller contact angle hysteresis¹⁹. Table 4 shows the roll-off angle data collected for the structures coated with the different hydrophobic films for the three general categories of features: micro-scale-only features (column called “No Nano”), nano-scale-only features (row called “No Micron”) and combined nano- and micro-scale.

Table 4. Roll-off angle in degrees for a 10 μ L water drop on PDMS, CYTOP and Teflon AF coated individual and combined nano-scale and micro-scale features. “P” indicates the drop was pinned and “>45” indicates the drop slides on the surface at an angle greater than 45° but less than 90°. Three measurements were made for each surface and the average value is reported here.

		Nano-scale Features (d/w)																								
		PDMS								CYTOP								Teflon AF								
		No Nano	Posts (1000/1000)	Iso Posts (2000/1000)	Iso Posts (3000/1000)	Posts (600/6000)	Iso Posts (1200/600)	Iso Posts (1800/600)	Posts (400/400)	No Nano	Posts (1000/1000)	Iso Posts (2000/1000)	Iso Posts (3000/1000)	Posts (600/6000)	Iso Posts (1200/600)	Iso Posts (1800/600)	Posts (400/400)	No Nano	Posts (1000/1000)	Iso Posts (2000/1000)	Iso Posts (3000/1000)	Posts (600/6000)	Iso Posts (1200/600)	Iso Posts (1800/600)	Posts (400/400)	
		No Micron	>45	P	P	P	P	9	P	P	32	16	5	P	>45	9	P	10	29	10	5	5	8	4	4	4
Micro-Scale Features (b/a)	No Micron	-	25	P	P	P	P	9	P	P	29	7	2	P	4	2	P	5	37	9	6	>45	7	5	3	4
	Checkerboard-1 (20/60)	-	18	P	P	P	20	7	>45	7	30	10	P	>45	7	3	P	10	37	7	4	>45	5	18	5	2
	Checkerboard-2 (20/40)	-	11	P	P	P	10	P	P	17	28	9	P	>45	14	P	P	22	33	7	5	P	6	4	3	3
	Checkerboard-3 (20/20)	-	P	P	P	P	P	P	P	>45	30	>45	P	>45	>45	P	>45	>45	>45	32	35	36	34	33	38	31
	Checkerboard-4 (40/20)	-	P	P	P	P	P	P	P	P	25	>45	>45	>45	36	>45	>45	38	>45	33	33	40	32	32	36	33
	Checkerboard-5 (60/20)	-	-	-	-	-	-	-	-	-	35	P	11	P	33	8	P	38	42	6	2	>45	4	2	P	2
	Checkerboard-6 (50/150)	-	17	P	P	P	16	9	P	11	33	10	9	>45	8	P	P	19	36	8	5	>45	5	3	6	6
	Checkerboard-7 (50/100)	-	14	P	P	P	17	P	P	>45	32	8	P	P	17	P	P	2	32	8	3	>45	5	3	>45	2
	Checkerboard-8 (50/50)	-	>45	P	P	>45	P	P	>45	>45	-	>45	>45	>45	>45	>45	>45	>45	30	35	29	36	35	31	>45	35
	Checkerboard-9 (100/50)	-	>45	>45	>45	>45	P	>45	>45	>45	-	P	>45	>45	>45	>45	P	>45	40	44	28	>45	33	30	32	32
Checkerboard-10 (150/50)	-	>45	>45	>45	>45	P	>45	>45	>45	-	P	>45	>45	>45	>45	P	>45	40	44	28	>45	33	30	32	32	

For a planar surface of grafted CYTOP, “No Micron” and “No Nano”, the roll-off angle for a 10 μ L drop was found to be $\phi = 32^\circ$. Assuming $\theta_{adv} \cong \theta_y$ equation 1 can be solved for θ_{rec} . The drop width was measured to be $x = 3.02$ mm and using $\gamma = 72$ mN/m, the receding angle was calculated to be $\theta_{rec} = 102^\circ$. This results in a contact angle hysteresis of $\Delta\theta = 14^\circ$. This closely matches the actual measured contact angle hysteresis from the advancing and receding angles ($\theta_{adv} = 118^\circ$, $\theta_{rec} = 106^\circ$, $\Delta\theta = 12^\circ$) for a planar surface of grafted CYTOP. Therefore surfaces fabricated in this study that produced contact angles $\geq 150^\circ$ with roll-off angles $\leq 10^\circ$ will be considered superhydrophobic.

Nano-scale square posts: Looking at only the nano-scale square post structures, several spacing-to-width ratio (d/w) combinations produced superhydrophobic surfaces, especially for the CYTOP and Teflon coated posts. Figure 2 shows the measured contact angle values plotted against the spacing-to-width ratio (d/w) for the 1000nm and 600nm nano-scale posts coated with CYTOP. Included are the

curves from the Wenzel and Cassie models. In the Wenzel state, the equilibrium contact angle θ_w is given by²¹

$$\cos \theta_w = r \cos \theta_y \quad (2)$$

where r is the roughness parameter and is the ratio of the total liquid-solid contact area to the surface area projected on the horizontal plane, and θ_y is the equilibrium angle on a planar surface (see “No Micron” and “No Nano” case in Table 3). For an array of square posts the expression for r is given by

$$r = 1 + \frac{4(h/w)}{(1+d/w)^2} \quad (3)$$

where h/w is the aspect ratio of the posts. For this study the post height, h was maintained constant at $h = 2\mu\text{m}$. In the Cassie state the water drop sits atop of the structure and contacts both solid and air. The equilibrium contact angle θ_c is given by²²

$$\cos \theta_c = f_{\text{SL}} \cos \theta_y - f_{\text{LA}} \quad (4)$$

where f_{SL} and f_{LA} are the fractions of the solid-liquid and liquid-air contact. For an array of square posts f_{SL} and f_{LA} are given by

$$f_{\text{SL}} = \frac{1}{(1+d/w)^2} : f_{\text{LA}} = 1 - \frac{1}{(1+d/w)^2} \quad (5)$$

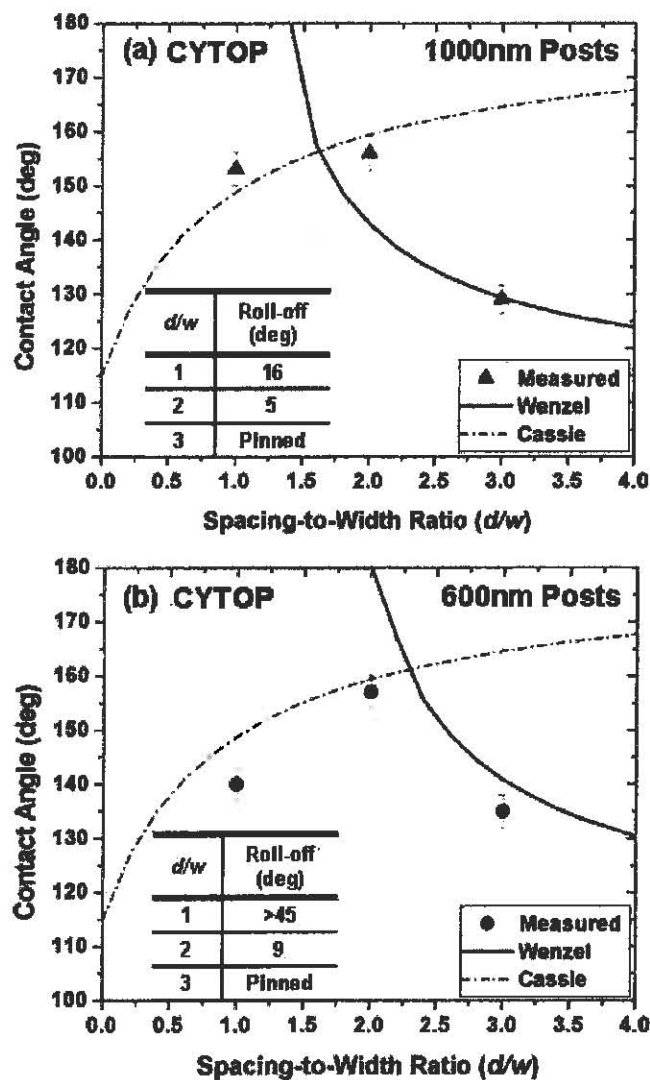


Figure 2. Measured contact angle of a 10 μ L drop of water on CYTOP coated nano-scale-only square post features with different spacing-to-width ratios (d/w). Included are the theoretical curves for the Wenzel and Cassie models. Also included are the drop roll-off angles for the different ratios. Plot (a) is for $w = 1000\text{nm}$ posts. Plot (b) is for $w = 600\text{nm}$ posts.

The contact angle data in the both plots in Figure 2 show that the drop appears to be in the Cassie state for $d/w \leq 2$, and appears to be in the Wenzel state for $d/w = 3$. Confirmation of these states is provided by measuring the roll-off angle, ϕ . For $d/w \leq 2$ the 10 μ L drop easily rolls from the surface confirming a Cassie state and for $d/w = 3$ the drop is pinned confirming the Wenzel state for both post sizes (1000nm and 600nm). In Figure 2, the point along the x-axis where the Cassie curve intersects with the Wenzel

curve indicates the minimum energy transition point favoring one state over the other. To the left of the intersection it is energetically favorable to be in the Cassie state and to the right it is energetically favorable to be in the Wenzel state. However, it is often seen that a drop can reside in a metastable state, where a Cassie state is observed when a Wenzel condition is predicted¹¹. This seems to be the case for the CYTOP-coated 1000 nm post having $d/w = 2$. It should be noted that neither the drop dispense rate nor the hydraulic pressure applied to the drop during dispense was systematically studied to see if these parameters could affect this observation.

As Figure 2 indicates the transition point, r_t , moved from $r_t = 1.5$ for 1000nm posts to $r_t = 2.25$ for 600nm posts. The position of this transition point not only can be controlled through geometry but also by the choice of hydrophobic coating. Figure 3 plots the measured contact angle values plotted against the spacing-to-width ratio (d/w) for the 600nm nano-scale posts for both PDMS and Teflon AF coated surfaces.

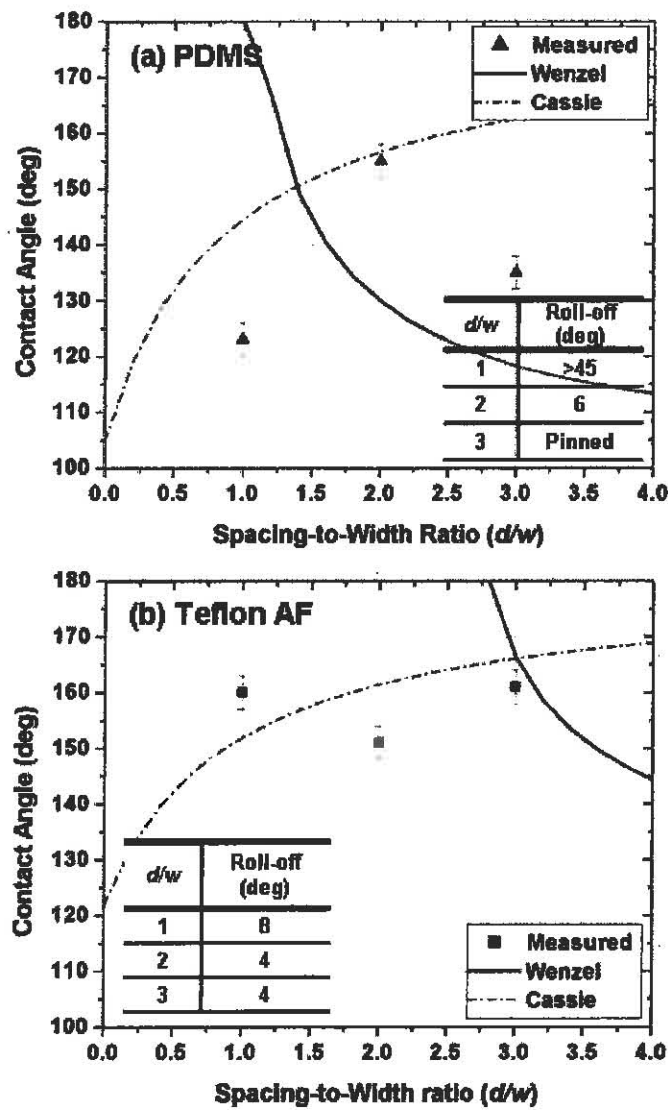


Figure 3. Measured contact angle of a $10\mu\text{L}$ drop of DI water on the nano-scale-only 600nm square post features with different spacing-to-width ratios (d/w). Included are the theoretical curves for the Wenzel and Cassie models. Also included are the drop roll-off angles for the different ratios. Plot (a) is for PDMS coated nano-scale posts and plot (b) is for Teflon AF coated nano-scale posts.

Comparing the different films, using the 600nm square posts as an example, the transition point is predicted to be $r_t = 1.4, 2.2$, and 3 for PDMS, CYTOP and Teflon AF respectively. This shift in transition point correlates to the surface energy of each film; the higher the surface energy of the film the smaller the spacing-to-width ratio before the transition from Cassie to Wenzel for a given geometry.

Table 5 compares the surface energy, contact angle and roll-off angle for planar surfaces coated with the different hydrophobic films investigated in this study.

Table 5. Surface energy, contact angle and roll-off angle for planar surfaces coated with different hydrophobic films. The roll-off angle, ϕ , measured using a 10 μL drop.

Coating	γ_s (mJ/m ²)	θ_y (deg)	ϕ (deg)
PDMS	22	105	>45
CYTOP	19	116	32
Teflon AF	16	122	29

In Figure 3a, the roll-off angle measurement for PDMS coated 600nm square posts for $d/w = 2$ indicates the drop was in a metastable Cassie state even though the Wenzel state is predicted. In the case of Teflon AF-coated 600nm square posts, the roll-off angles were measured to between 4° and 8° for the three different d/w ratios indicating the drop was in the Cassie state for all the different post spacings. In addition, the contact angles measured for the three different d/w ratios were $>150^\circ$, and this coupled with the low roll-off angle ($\phi < 10^\circ$), by definition means the combination of Teflon AF and 600nm nano-scale square posts created a superhydrophobic surface. This is a clear example that a superhydrophobic surface can be produced using a single-length-scale structure and low energy hydrophobic film.

Micro-scale Checkerboards: The results for the micro-scale only checkerboard structures were not much different than for a planar surface, suggesting the height of the structures relative to feature width was not sufficient to enhance the wetting state. Since the height of the structures was only 2 μm and the micro-scale structures were $\geq 20\mu\text{m}$ the roughness term in the Wenzel equation was approximately $r = 1$ for each checkerboard design. The one exception was the checkerboard pattern for $b/a = 1$ which produced contact angles significantly higher in some cases than the planar case for each film. To gain insight, a visualization technique adopted by Ralston *et. al.*²³ was used in which the drop was sandwiched between the hydrophobic surface and glass slide having a higher surface energy thereby

allowing for a the contact line to be directly observed. Figure 4 shows a portion of the advancing water contact line on the surface of the micro-scale checkerboard feature for $b/a = 0.5, 1$ and 2 .

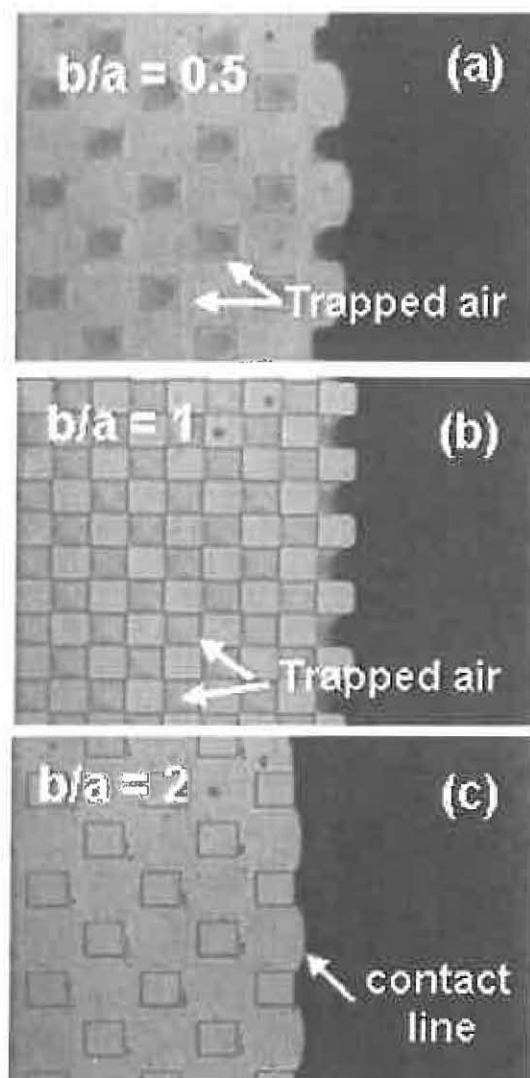


Figure 4. Image showing a portion of the three phase contact line of a water drop on the micro-scale-only checkerboard structures coated with CYTOP for $b/a = 0.5, 1$ and 2 . For $b/a \leq 1$, Figure 4(a) and Figure 4(b) air is trapped in the etch pockets (denoted by the different gray of surface) and for $b/a > 1$, Figure 4(c) the water drop is in complete contact with the surface. Image made by sandwiching the drop between the micro-scale surface and a glass slide. Since the textured surface is more hydrophobic than the glass slide, the three phase contact line at the surface can be directly viewed.

The images show that for $b/a \leq 1$ air is trapped in the etched pockets, as indicated by the gray scale color difference on the surface. Since the drop contacts both solid and air by definition it is in a Cassie state. For $b/a > 1$ the image shows no trapped air meaning the drop is in direct contact with the entire surface indicating a Wenzel state. An interesting observation was for the micro-scale-only checkerboards having $b/a > 1$ a 10 μ l drop still rolled off the surface for the CYTOP coated and Teflon AF coated surfaces even though the drop was clearly in a Wenzel state. This was probably due to the fact the height is only 2 μ m and thus can not create enough pinning force along the interface. Thus, a water drop in Wenzel state does not necessarily have to be pinned.

Nano-scale posts patterned into micro-scale checkerboard shapes: Results from patterning the nano-scale square posts into micro-scale checkerboard shapes indicate when the checkerboard spacing-to-width ratio was $b/a > 1$ the micro-scale checkerboard features dominate the wetting state independent of the nano-scale feature. The measured contact angles and roll-off angles were similar to micro-scale-only checkerboard results for $b/a > 1$. An interesting observation was the water interface over the nano-scale posts for these checkerboard features showed behavior identical to the water interface for the corresponding nano-scale-only feature, meaning if it was in a Cassie state for nano-scale-only, the interface over the posts for the combined features was also in a Cassie state. Figure 5 shows a portion of the water contact line on the surface of micro-scale checkerboard feature for $b/a = 3$ for two different 1000nm posts spacing-to-width ratios coated with CYTOP. The image in Figure 5(a) shows the water interface resting on top of the 1000nm posts having a $d/w = 1$, but contacting the surface between the islands of nano-posts demonstrating a combination Cassie-Wenzel condition. In Figure 5(b) the 1000nm posts have a $d/w = 3$ and the water interface is contacting all surfaces indicating a Wenzel only condition.

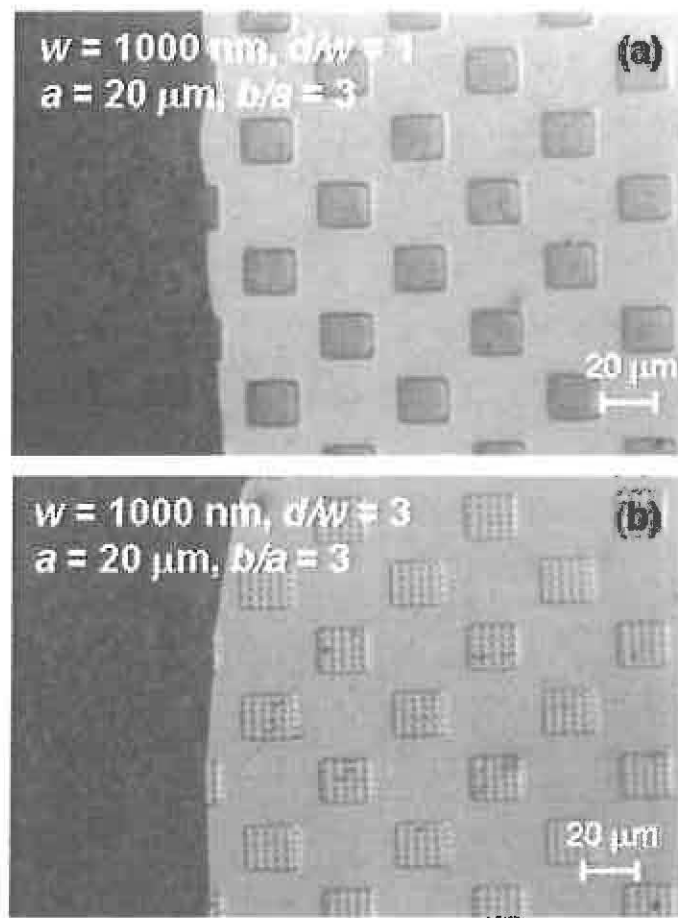


Figure 5. Image showing a portion of the three phase contact line of a water drop on the combination micro-scale checkerboard structures for $a = 20\mu\text{m}$ and $b/a = 3$ and the $w = 1000\text{nm}$ posts with different d/w ratios coated with CYTOP. (a) For $d/w = 1$ the water interface is on top of the nano-post (denoted by the different gray of surface) and in contact with surface between the groups of nano-posts indicating a combination Cassie-Wenzel condition. (b) For $d/w = 3$ the water interface is in complete contact with the surface indicating a Wenzel condition. Image made by sandwiching the drop between the micro-nano scale surface and a glass slide. Since the textured surface is more hydrophobic than the glass slide, the three phase contact line at the surface can be directly viewed.

Results for the combination nano-scale and micro-scale surfaces having micro-scale checkerboard patterns $b/a \leq 1$ shows the wetting state to be influenced by both length-scale structures. Based on measured contact angles and roll-off angles, the combinations of micro-scale checkerboards having b/a

≤ 1 with nano-scale posts having $d/w = 1$ actually increased the hydrophobicity and lowered water adhesion of the surface compared to a surface with just nano-scale-only posts. The surfaces coated with PDMS showed the greatest increase in hydrophobicity due to this nano- and micro-scale combination. The reason PDMS coated surfaces were affected more is connected to the surface energy of the film (Table 5). As presented earlier, CYTOP and Teflon AF coated nano-scale-only posts for $d/w = 1$ created superhydrophobic surfaces having contact angle $>150^\circ$ and roll-off angles $<20^\circ$. Thus when these surfaces were patterned into micro-scale checkerboards ($b/a \leq 1$) the positive effect of this combination was not as noticeable. Unlike with PDMS, which has a higher surface energy than CYTOP or Teflon AF, it produced a less hydrophobic surface with nano-scale-only posts and thus appears to be more affected by changes in length scale.

Conversely, a different effect was seen for nano-scale posts having spacing-to-width ratios $d/w > 1$ patterned into micro-scale checkerboards with $b/a \leq 1$. At this sizing, the micro-scale features adversely affected the hydrophobicity of the surface, as compared to the nano-scale-only surface. This indicates that as the spacing between the nano-scale posts grows, combined with large sections of post being removed for the substrate, it becomes more energetically favorable for a drop to transition from a Cassie state to the Wenzel state. This behavior trend has also been observed on hierarchy structures⁹ where it was observed that the larger the spacing of the micro-scale structures, the lower the hydrophobicity of the surface.

Wenzel and Cassie models were developed to understand this behavior. The roughness parameter, r , in the Wenzel equation (Eq. 2) and area fractions, f_{SL} and f_{LA} in the Cassie equation (Eq. 4) are different for each micro-scale checkerboard spacing-to-width ratio. In this communication we will limit the analysis to the checkerboard pattern $b/a = 1$. The expression for r for nano-scale posts patterned into a micro-scale checkerboard pattern having $b/a = 1$ becomes:

$$r = 1 + \frac{wh(4n - m)}{2a^2} \quad (6)$$

where m is the number of posts along length a , and n is the number of posts in an area of $a \times a$. For the Cassie model, the solid-liquid, f_{SL} and liquid-air fractions, f_{LA} for this surface becomes:

$$f_{SL} = \frac{nw^2}{2a^2} : f_{LA} = 1 - \frac{nw^2}{2a^2} \quad (7)$$

As expected, both the Cassie and Wenzel models are functions of the number of nano-posts contained in the micro-scale pattern. Figure 6 shows a plot of solutions to the Wenzel and Cassie models using equations 6 and 7, for 600 nm square posts and the micro-scale checkerboard pattern $b/a = 1$ coated with CYTOP. Included in the plot are the Wenzel and Cassie solutions for the nano-scale-only square posts. The jagged shape to the Wenzel and Cassie curves is a direct result of maintaining a whole number of nano-posts within a fixed micro-scale pattern.

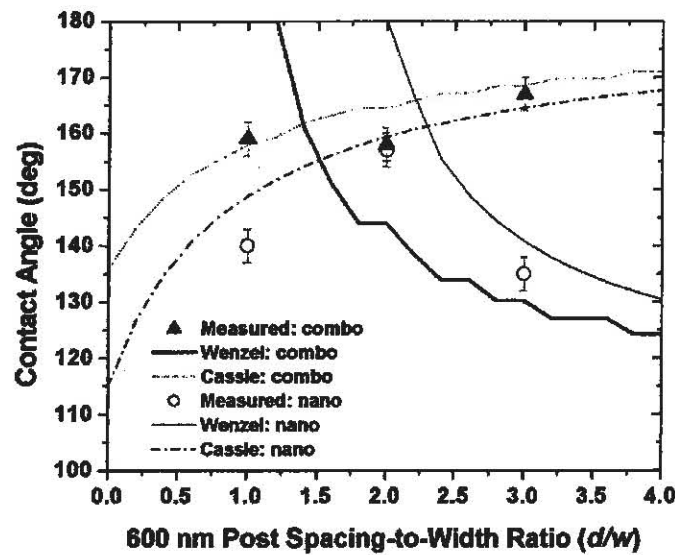


Figure 6. Wenzel and Cassie model solutions for the combined nano-scale square posts with different d/w ratios for $w = 600\text{nm}$ and the micro-scale checkerboard pattern $b/a = 1$ for $a = 20\mu\text{m}$ coated with CYTOP (referred to in the figure as “combo”). Included are the Wenzel and Cassie model solutions for the nano-scale-only square posts (referred to in the figure as “nano”). Also included are the measured contact angles for both sets of surfaces.

As the Cassie model in Figure 6 shows, and data supports, the hydrophobicity of the surface increases for combinations of micro-scale checkerboards for $b/a \leq 1$ with nano-scale posts having $d/w \leq 1$, compared to the nano-scale-only surface of similar spacing-to-width ratios. However, combining the nano-scale and micro-scale features together cause the transition from Cassie to Wenzel to occur at smaller spacing-to-width ratios as compared to a surface with only nano-scale posts. This points to why water drops were pinned on the combined surfaces having $d/w > 1$ compared to the nano-scale-only surface of equal spacing-to-width ratios. This general behavior also trends with the other nano-posts sizes tested.

Even though the measured contact angles for the combined case with $d/w = 2$ and 3 were high and appeared to track with the Cassie model (Figure 6), the drops for each surface were actually in the Wenzel state as evident of water drops being pinned during the roll-off angle measurement (see Table 4). These high contact angles are attributed to the interface being pinned not only among the nano-posts, but also along the micro-scale checkerboard pattern as shown in Figure 4(b).

Similar behavior was seen for the PDMS and Teflon AF coated surfaces where the hydrophobicity of the surface increases for combinations of micro-scale checkerboards for $b/a \leq 1$ with nano-scale posts having $d/w \leq 1$, compared to the nano-scale-only surface of similar spacing-to-width ratios. Figure 7 is a plot of solutions to the Wenzel and Cassie models using equations 6 and 7, for 600 nm square posts and the micro-scale checkerboard pattern $b/a = 1$ for PDMS and Teflon AF coated surfaces. The geometry changes appear to have a greater effect for the PDMS coated surfaces than for Teflon AF coated surfaces. As mentioned previously, this has to do with the surface energy of each film. The low surface energy of Teflon AF, compared to the other films investigated, must be enough to leave a 10 μ L drop of water in the Cassie state for the different post spacing-to-width ratios independent of the patterning i.e. nano-scale posts only or combined micro-scale checkerboards.

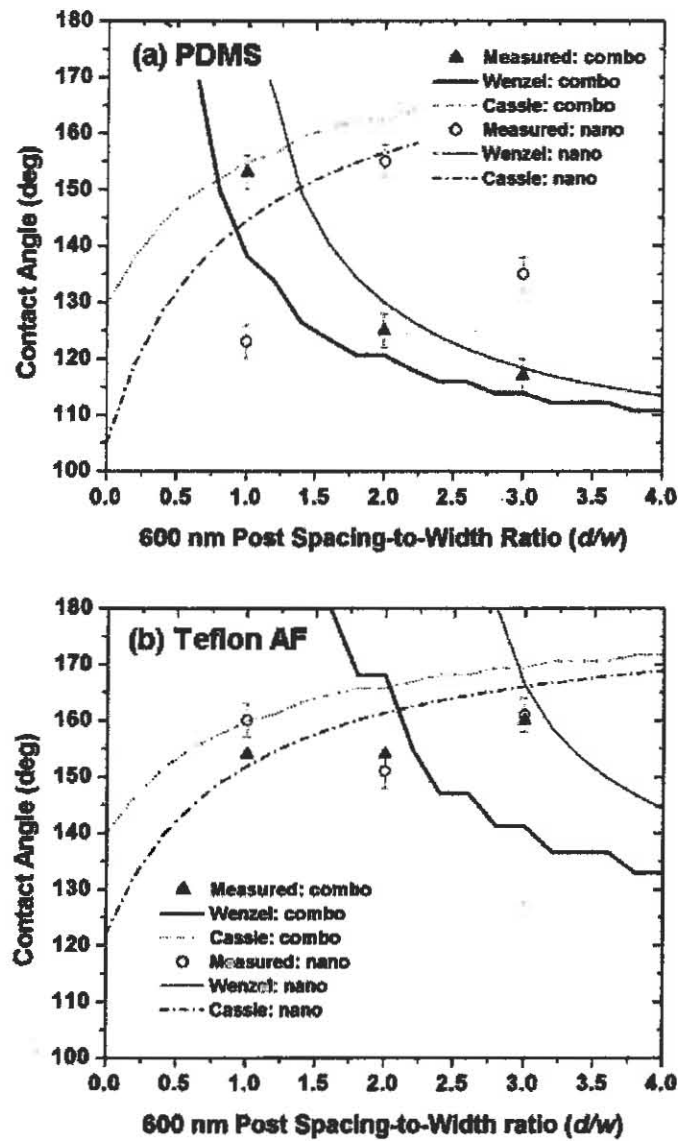


Figure 7. (a) Wenzel and Cassie model solutions for the combined nano-scale square posts with different d/w ratios for $w = 600\text{nm}$ and the micro-scale checkerboard pattern $b/a = 1$ for $a = 20\mu\text{m}$ coated with PDMS (referred to in the figure as “combo”). Included are the Wenzel and Cassie model solutions for the nano-scale-only square posts (referred to in the figure as “nano”). Also included are the measured contact angles for both sets of surfaces. (b) Wenzel and Cassie model solutions for the combined nano-scale square posts with different d/w ratios for $w = 600\text{nm}$ and the micro-scale checkerboard pattern $b/a = 1$ for $a = 20\mu\text{m}$ coated with Teflon AF (referred to in the figure as “combo”). Included are the Wenzel and Cassie model solutions for the nano-scale-only square posts (referred to in the figure as “nano”). Also included are the measured contact angles for both sets of surfaces.

Summary

In this study we looked at the effect a heterogeneous surface consisting of nano-scale square posts patterned in micro-scale checkerboard shapes had on surface hydrophobicity. Our results indicate that it was possible to increase both surface hydrophobicity as well as lower surface hydrophobicity using a heterogeneous surface depending the ratio of feature sizes compared to a continuous surface made of either all nano-scale or all micro-scale structures. For nano-scale posts with spacing-to-width ratios, $d/w \leq 1$ patterned into micro-scale checkerboards shapes with spacing-to-width ratios, $b/a \leq 1$, surface hydrophobicity increased compared to a nano-scale-only surface with the same spacing-to-width ratio. Our results also show that the transition from a Cassie state to a Wenzel state occurs at smaller nano-scale spacing-to-width ratios for combined nano-scale, micro-scale surfaces compared to the nano-scale-only surface. The findings from this study also show how critical surface modifications can be for achieving a superhydrophobic state for a fixed geometry. Depending on the surface energy of solid, a fixed surface roughness that exhibits high adhesion and low hydrophobicity can also exhibit low adhesion and superhydrophobicity by changing the surface coating.

Acknowledgment. The authors thank Dolores Shibbes for taking the scanning electron microscope images of the different surfaces fabricated in this study. This work was sponsored by the Department of the Air Force under Air Force Contract FA8721-05-C-0002. Opinions, interpretations, conclusions, and recommendations are those of the authors, and do not necessarily represent the view of the United States Government.

REFERENCES

- (1) Zorba, V.; Stratakis, E.; Barberoglou, M.; Spanakis, E.; Tzanetakis, P.; Anastasiadis, S.; Fotakis, C. *Adv. Mater.* **2008**, *20*, 4049.
- (2) Feng, L.; Zhang, Y.; Xi, J.; Zhu, Y.; Wang, N.; Xia, F.; Jiang, L. *Langmuir* **2008**, *24*, 4114-4119.
- (3) Bormashenko, E.; Bormashenko, Y.; Stein, T.; Whyman, G.; Bormanshenko, E. *J. Coll. Inter. Sci.* **2007**, *311*, 212-216.
- (4) Watson, G. S.; Watson, J. A. *Applied Surface Science* **2004**, *235*, 139-144.
- (5) Ma, M.; Hill, R. M. *Current Opinion Coll. Inter. Sci.* **2006**, *11*, 193-202.
- (6) Bhushan, B.; Koch, K.; Jung, Y. C. *Applied Physics Letters* **2008**, *93*, 093101.
- (7) Ming, W.; Wu, D.; van Benthem, R.; de With, G. *Nano Letters* **2005**, *5*, 2298-2301.
- (8) Wagterveld, R. W.; Berendsen, W. J.; Bouaidat, S.; Jonsmann, J. *Langmuir* **2006**, *22*, 10904-10908.
- (9) Lee, Y.; Park, S. H.; Kim, K. B.; Lee, J. K. *Advanced Materials* **2007**, *19*, 2330-2335.
- (10) Yeh, K. Y.; Chen, L. J.; Chang, J. Y. *Langmuir* **2008**, *24*, 245-251.
- (11) Varanasi, K. K.; Deng, T.; Hsu, M. F.; Bhate, N. *Proceedings of IPACK2009*; San Francisco, California, 2009.
- (12) Dorrer, C.; Rühe, J. *Langmuir* **2006**, *22*, 7652-7657.
- (13) Cao, L.; Hu, H. H.; Gao, D. *Langmuir* **2007**, *23*, 4310-4314.
- (14) Martines, E.; Seunarine, K.; Morgan, H.; Gadegaard, N.; Wilkinson, C.; Riehle, M. *Nano Letters* **2005**, *5*, 2097-2103.

- (15) Ahuja, A.; Taylor, J. A.; Lifton, V.; Sidorenko, A. A.; Salmon, T. R.; Lobaton, E. J.; Kolodner, P.; Krupenkin, T. N. *Langmuir* **2008**, *24*, 9-14.
- (16) Wu, J.; Xia, J.; Lei, W.; Wang, B. P. *Applied Physics A* **2010**, *99*, 931-934.
- (17) Burton, Z.; Bhushan, B. *Nano Letters* **2005**, *5*, 1607-1613.
- (18) Travana, H.; Amirfazli, A.; Neumann, A. W. *Langmuir* **2006**, *22*, 5556-5559.
- (19) Öner, D.; McCarthy, T. J. *Langmuir* **2000**, *16*, 7777-7782.
- (20) Chen, W.; Fadeev, A. Y.; Hsieh, M. C.; Öner, D.; Youngblood, J.; McCarthy, T. J. *Langmuir* **1999**, *15*, 3395-3399.
- (21) Wenzel, R. N. *Ind. Eng. Chem.* **1936**, *28*, 988-994.
- (22) Cassie, A. B. D. ; Baxter, S. *Trans. Faraday Soc.* **1944**, *40*, 546-551.
- (23) Priest, C.; Albrecht, T. W. J.; Sedev, R.; Ralston, J. *Langmuir* **2009**, *25*, 5655-5660.